ISBN: 978-3-95450-247-9 ISSN: 2673-5490 doi: 10.18429/JACoW-IPAC2024-THXN1

HIGH GRADIENT RF PHOTOINJECTOR AT LANL*

A. Alexander†, P. M. Anisimov, W. Barkley, D. Dimitrov, T. P. Grumstrup, B. Haynes, C. Huang, D. Perez, R. Shinohara, E. I. Simakov, G. Wang, H. Xu, J. Zhang, M. Zuboraj
Los Alamos National Laboratory, Los Alamos, NM, USA

Abstract

This work summarizes recent results from the Cathodes And Radio-frequency Interactions in Extremes (CARIE) project. The C-band, 5.712 GHz klystron and modulator have been installed and conditioned at high power. Low power RF measurements have been performed on the plug-free injector and the injector has been tuned. The RF design of an injector that integrates a high QE cathode has been completed, and engineering design is underway. Simulations of the injector's beam dynamics were performed, and the cathode specifications maximizing brightness and minimizing emittance have been determined using a MOGA algorithm. CsTe has been selected as an initial high QE photocathode material. An ab-initio model predicting key materials parameters for CsTe has been developed. Two photoemission models (Monte Carlo and 3-step) have been developed to predict the QE of the photocathode, with plans to describe more beam parameters in the future. CsTe photocathodes have been grown and characterized, and fabrication has begun on the vacuum suitcase that will transport them from the growth chamber to the photoinjector. High QE photocathode testing at high gradients is planned in 2025.

INTRODUCTION AND PROJECT GOALS

The Cathodes And Radio-frequency Interactions in Extremes (CARIE) project at Los Alamos National Laboratory (LANL) in New Mexico, USA will test performance of high quantum efficiency (QE) photocathodes in a high-gradient photoinjector. The project's ultimate goal is to deploy this technology for an inverse Compton scattering (ICS) or ultrafast electron diffraction (UED) capability at LANL. The key photoinjector performance requirements include:

- 250 pC bunch charge
- 240 MV/m peak field at the cathode
- 100 nm emittance

SYSTEM DESIGN

The experimental test stand under construction will include of a high power 5.7 GHz RF system comprised of a klystron, a modulator,waveguides, and a circulator. A photoinjector will produce an electron beam from a high-QE cathode and accelerate it to 7 MeV in a 1.6-cell RF structure. The photocathode grown on a metal plug face will be mounted in the photoinjector, with plug transport and handling conducted at ultra-high vacuum (UHV) conditions at all times in a suitcase and two load locks. A solenoid magnet immediately downstream of the photoinjector is designed for emittance compensation. Extensive beam diagnostics are planned.

HIGH POWER RF SYSTEM

A conceptual schematic of the high power RF system is shown in Fig. 1.

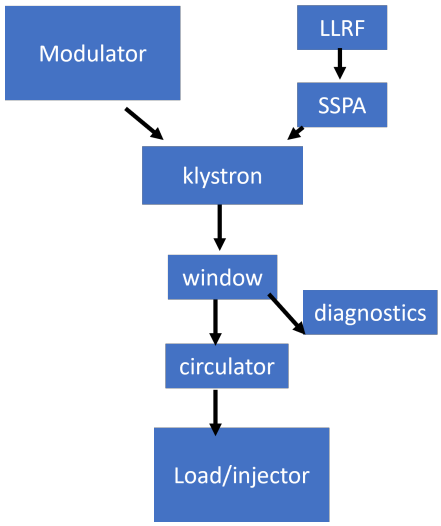

Figure 1: High power RF system diagram.

Key components of the RF system include the klystron with a modulator, and the circulator for minimizing damage to the klystron from RF reflections. The klystron has been conditioned to 35 MW into a dummy load. The maximum achieved RF powers and repetition rates can be seen in Table 1. We were unable to condition the klystron to the maximum factory-specified power of 50 MW due to the limited cooling capacity of the chiller [1]. However, demonstrated powers are still much greater than the maximum power needed by the injector (about 10 MW). The circulator is currently being installed. The circulator is a relatively new design, theoretically rated for 50 MW peak power and 5 kW average RF power when filled with SF6 at 345 kPa (50 psig). The circulator has not yet been tested to high power. Should the circulator fail to perform at full power, it will be replaced with a magic-tee.

C-BAND INJECTOR DESIGN

We have designed two injectors. One design is plug-free and is shown in Fig. 2. This design focuses on the tuning and high gradient testing of the RF cavity without a high QE photocathode or plug [2]. The design is very similar to

* Work supported by Los Alamos National Laboratory's Laboratory Directed Research and Development (LDRD) Program, project 20230011DR
† aalexander@lanl.gov

ISBN: 978-3-95450-247-9 ISSN: 2673-5490 doi: 10.18429/JACoW-IPAC2024-THXN1

Table 1: Klystron Conditioning Results for Three Pulse Widths

Freq. (Hz)	1.00 µs	1.25 µs	1.50 µs
1	36 MW	36 MW	36 MW
20	NA	36 MW	36 MW
40	NA	25 MW	20 MW

the plug-insert design, as shown by the RF parameters in Table 2 . The design uses a solid Cu backplane and thus a Cu photocathode instead of a plug, and has less symmetry due to being an earlier design. A picture of the fabricated injector before brazing is shown in

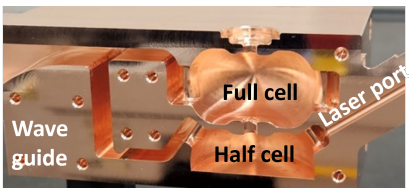

Figure 2: The plug-free photoinjector before brazing

Plug Insert Design Overview

The second photoinjector design incorporates a removable plug for incorporating high QE photocathodes. Two views of the plug-insert injector are shown in Figs. 3 and 4.

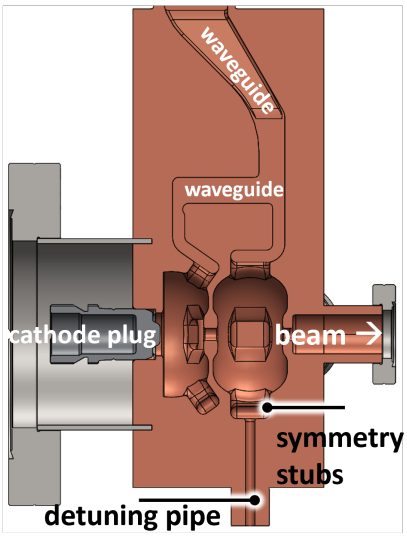

Figure 3: Longitudinal cross-section with a vertical cut of the plug-insert photoinjector.

The design has several important features to symmetrize the RF fields for emittance reduction. There are three symmetry stubs in the cathode cell and in the full cell, respectively, designed for minimizing the dipole RF content induced by the RF coupling slot at the top in each cell. In the cathode cell, on the outer faces of the two symmetry stubs on the horizontal plane, laser pipes are opened. This design allows

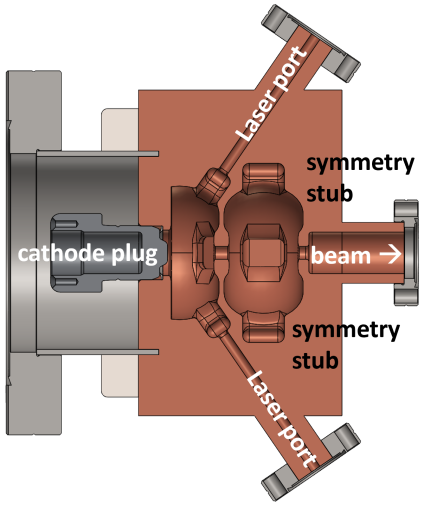

Figure 4: Horizontal Longitudinal cross section with a horizontal cut of the plug-insert photoinjector.

the laser, when reflected by the photocathode film, to exit the cavity without being scattered inside the cathode cell. The key beam parameters for the plug free and plug insert design are compared in Table 2.

Table 2: Injector Design Parameters

Design Parameter	Plug Free	Plug-insert
Quality Factor, Q	11934	11571
Full Cell Shunt Impedance (MΩ)	3.09	3.09
Power for 100 MV/m field on cathode (MW)	1.7	1.8
Power for 240 MV/m field on cathode (MW)	9.5	10.4

It can be seen that the parameters are very similar, though the Q factor for the design with a plug insert is lower. The plug design is based on the INFN plug. , The plug tip geometry was designed to provide a uniform cathode fields while minimizing the multipactor. An analysis of the injector's peak RF fields was performed. The peak magnetic field is on the symmetry stubs, while the peak electric fields is on the re-entrant features. The peak electric field on the photocathode is ~75-80% of field on the re-entrant features and plug edges [3].

Low Power RF Tests

The plug-free injector has been fabricated. The plug free injector was designed at the end of 2022 and fabricated in 2023.

We performed low-power RF measurements on the plug copper injector and tuned the RF cavity to achieve a balanced field distribution at 5.712 GHz. In addition to S11 measurements, we have also performed a bead drop measurement, which is similar to a bead pull measurement except that the

ISBN: 978-3-95450-247-9 ISSN: 2673-5490 doi: 10.18429/JACoW-IPAC2024-THXN1

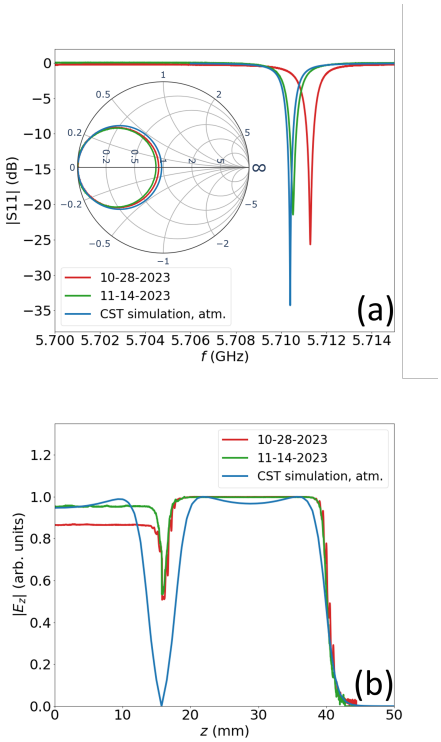

Figure 5: Low power test results of (a) S11 measurements and (b) bead drop measurements, compared to the results from CST simulations of the injector in atmosphere.

bead cannot be pulled through the cavity due to the solid photocathode back plane. These results are shown in Fig. 5. Our tuning was successful and our results are in agreement with CST simulations.

Beam Dynamics Results

We conducted extensive beam dynamics simulations with GPT to maximize theelectron beam brightness and minimize emittance. Seven parameters were considered:

- solenoid position,
- solenoid magnetic field strength,
- RF launching phase,
- electron spot size,
- spatial electron uniformity,
- electron bunch length,
- electron temporal uniformity.

There are several main conclusions from these investigations: first, as seen in Fig. 6, the 2024 design is a significant improvement over the 2022 and 2023 designs. Second, the 2024 design results in an optimal bunch length that is substantially smaller (70% of previous designs). Third, as shown in Ref. [4], the laser and photocathode requirements are extremely stringent: the spatial electron beam profile is essentially flat top, and the beam rise time is extremely sharp. The simulations also assume 5 meV mean transverse energy (MTE), although it is possible that the effect of increased MTE is minimal so long as it is below a relatively large threshold, as was previously found in Ref. [5].

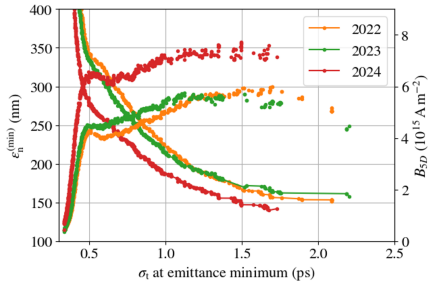

Figure 6: Emittance and brightness as a function of bunch length.

PHOTOCATHODE MODELS

Substantial work has gone toward developing models to predict photocathode performance at high gradients. In particular, the (wavelength and temperature dependent) efficiency, MTE, response time, and breakdown voltage. They are essentially transient semiconductor device models, similar to those developed by the transistor and solar cell communities. A key difference is that the UHV conditions required for photocathode integrity means that many typical materials parameters have not been measured. As a result, we have used ab initio based models, in particular using DFT to estimate unknown materials parameters for the photoemission and breakdown models.

We developed two photoemission model types to predict photocathode behavior, one three-step model and one Monte Carlo model. The key distinction between them is the three-step model assumes the energy of an electron decays exponentially with distance from the photocathode surface due to phonon interactions, while the Monte Carlo explicitly models the electron transport and scattering as a random process.

Ab-initio Materials Model

Previously, we used DFT to estimate the optical properties and density of states (DoS) of cesium-two telluride (Cs_2Te).

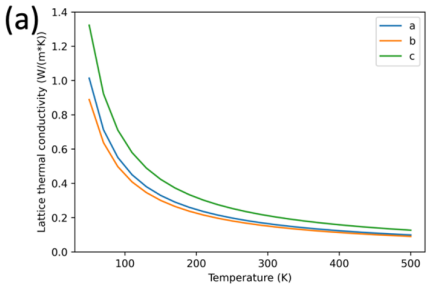

Figure 7: Thermal conductivity of Cs_2Te from DFT.

More recently, we have simulated the mobility, and electrical and thermal conductivity of Cs_2Te, which are shown in Figs. 7 and 8. Our results show particularly poor thermal and electrical conductivity, likely due to the ionic nature of Cs_2Te [6].

ISBN: 978-3-95450-247-9 ISSN: 2673-5490 doi: 10.18429/JACoW-IPAC2024-THXN1

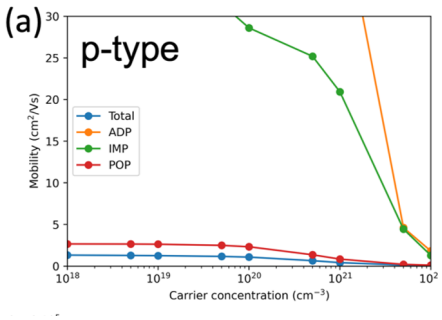

Figure 8: Electron mobility of Cs_2Te from DFT.

Three-Step Photoemission Model

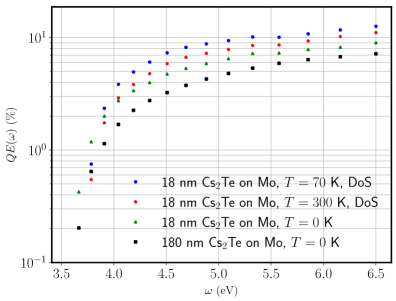

Figure 9: QE of Cs_2Te vs energy and temperature.

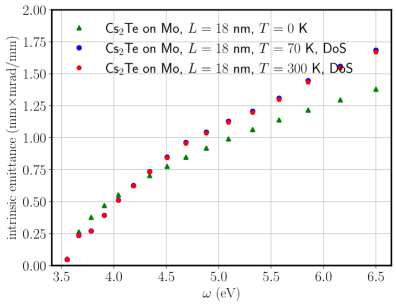

Figure 10: Emittance of Cs_2Te vs energy and temperature.

Previously, we used Cs_3Sb to experimentally validate our model and demonstrated optical interference effects. Our more recent work incorporates a finite temperature and more realistic DoS, derived from the DFT simulations of Cs_2Te [7]. Figures 9 and 10 show increasing QE and emittance with temperature, which is consistent with existing theoretical and experimental work.

Monte Carlo Photoemission Model

The Monte Carlo models have largely focused on the effects of gradients on electron transport. Figure 11 shows the QE enhancement due to film thickness and gradient, with both curves normalized to a 200 nm thick Cs_2Te photocathode with no applied electric field [8]. Even relatively low electric fields can substantially enhance QE, due to both the

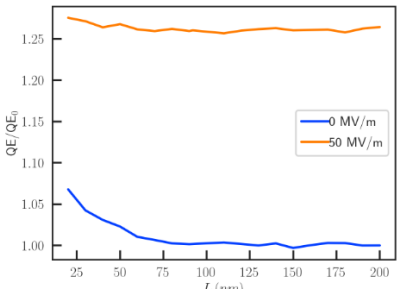

Figure 11: QE enhancement vs a infinitely thick Cs_2Te cathode with no applied electric field.

ability of the applied electric field to "turn around" electrons moving toward the backside of the photocathode, and to offset energy losses from phonons by accelerating the electrons in the conduction band toward the surface.

Breakdown Models

There are multiple approaches to modelling material breakdown in high fields. In particular, metal-based breakdown models typically focus on mechanical deformation and field emission, while semiconductor models assume perfectly smooth surfaces and model effects such as avalanche breakdown. We are developing both styles of models, with an eventual goal of integrating them.

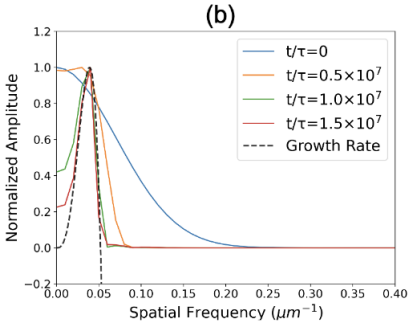

Figure 12: Characteristic length scale of surface features assuming 48 K temperature rise, 192 MV/m applied gradient, and 0.1 initial aspect ratio.

Our most recent metal breakdown model, shown in Fig. 12 finds that when both an electric field and temperature rise (e.g. from Joule heating) are applied, the surface features reorganize with a characteristic length scale that depends both on the applied field and temperature difference.

Our semiconductor breakdown model assumes a perfectly smooth, infinitely thick material and uses the applied electric field and phonon information to develop rates of energy gain and energy loss for an electron. A material is assumed to undergo breakdown when the energy gain rate (for a given electric field) is higher than the loss rate produced from phonons, where the phonon information has been derived from DFT.

ISBN: 978-3-95450-247-9 ISSN: 2673-5490 doi: 10.18429/JACoW-IPAC2024-THXN1

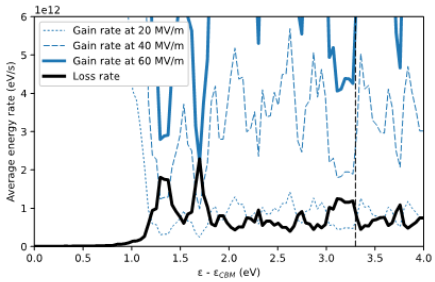

Figure 13: Breakdown rate predicted from phonon loss.

This model, shown in Fig. 13 predicts that Cs_2Te should break down at 35 MV/m. However, there are factors that may delay breakdown. First is the finite thickness of the material, which may enable photoemission or more extensive losses at the vacuum/substrate interface, rather than producing a breakdown event. This work also suggests that additional loss mechanisms could help prevent breakdown, and suggest that the imperfect materials currently being used may have some enhanced, uncharacterized breakdown resistance. We are planning to incorporate these effects into our Monte Carlo model to better understand tradeoffs between breakdown strength and thickness and material quality.

PHOTOCATHODE GROWTH

We have recently started to grow CsTe photocathodes. While we have fabricated photocathodes using both sequential and copdeosition, we intend to use a codeposition process for the photocathodes used in CARIE , both to keep QE high and the geometric contribution to the emittance low.

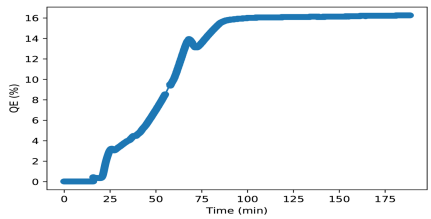

Figure 14: QE of CsTe during growth.

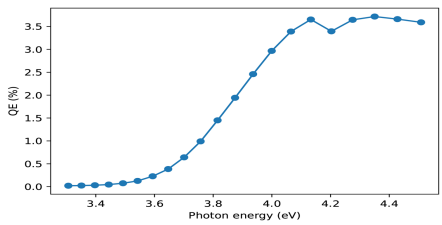

Figure 15: Spectral Response (QE) of CsTe after photocathode growth and cooling to room temperature.

We successfully grew high QE photocathodes, as seen in Fig. 14. However, we are still working to refine our photocathode growth turn off and cooling process. Figure 15 shows a typical spectral response after terminating the growth and letting the cathode cool to room temperature [9].

PHOTOCATHODE TRANSPORT

High QE semiconductor photocathodes must be transported under UHV conditions (~10^{-10} Torr) in order to preserve their properties. We have completed the design of our vacuum suitcase which will transportphotocathode plugs between our growth system and injector. We have also completed most of the modifications to our existing growth chamber to accomomdate our vacuum suitcase, and have a preliminary design of the load lock for the photoinjector.

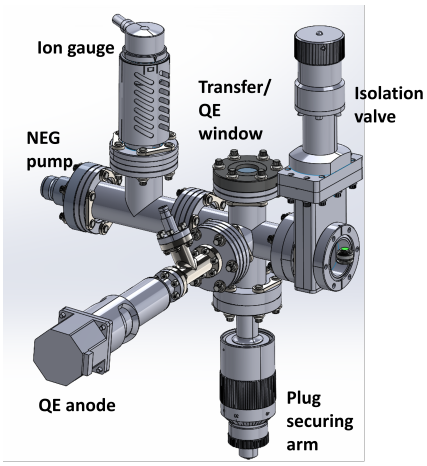

Figure 16: CAD model of the CARIE vacuum suitcase.

Figure 16 shows a CAD model of the CARIE vacuum suitcase. It is designed to be carried by a single person, with/ minimal vacuum diagnostics and pumping (passive NEG only) to keep the weight low and the system easy to handle. The 2.75" flange is only large enough for the ACERT-style half-plug and not the full INFN style plugs [10]. However, this is acceptable as the LANL/ACERT growth system is already incompatible with the full sized INFN-style plug. However, the new photoinjector load lock will have an arm with interchangeable manipulators, which will permit use of the ACERT half plug, full sized INFN plug, and other plug systems.

FUTURE PLANS

We will perform high power tests on the plug-free injector in 2024. We expect to build the plug insert photoinjector and test (high QE) photocathodes in 2025.

REFERENCES

[1] E. Simakov *et al.*, "Status of the CARIE high gradient photocathode test facility at LANL", presented at the IPAC'24, Nashville, TN, USA, May 2024, paper WEPC60, this conference.

[2] H. Xu, P. Anisimov, W. Barkley, and E. Simakov, "C-band photoinjector radiofrequency cavity design for enhanced beam generation", in *Proc. IPAC'23*, Venice, Italy, May 2023,

ISBN: 978-3-95450-247-9 ISSN: 2673-5490 doi: 10.18429/JACoW-IPAC2024-THXN1

pp. 2061–2063.
doi:10.18429/JACoW-IPAC2023-TUPL139

[3] H. Xu *et al.*, "RF and multipactor analysis for the CARIE RF photoinjector with a photocathode insert", presented at the IPAC'24, Nashville, TN, USA, May 2024, paper THPG04, this conference.

[4] P. M. Anisimov *et al.*, "Multi-objective genetic optimization of high charge TopGun photoinjector", presented at the IPAC'24, Nashville, TN, USA, May 2024, paper MOPS55, this conference.

[5] P. M. Anisimov *et al.*, "Emittance compensation in a high charge TOPGUN photoinjector", in *Proc. IPAC'23*, Venice, Italy, May 2023, pp. 2747–2750.
doi:10.18429/JACoW-IPAC2023-WEPA042

[6] G. Wang *et al.*, "A first-principles study of structural, elastic, electronic, and transport properties of Cs2Te".
doi:10.48550/2405.04398

[7] D. Dimitrov *et al.*, "Temperature, density of states, and thin film optical effects on electron emission from semiconductor photocathodes", presented at the IPAC'24, Nashville, TN, USA, May 2024, paper WEPR67, this conference.

[8] C. Huang *et al.*, "Monte-Carlo photoemission model for thin film semiconductors under high fields", presented at the IPAC'24, Nashville, TN, USA, May 2024, paper WEPC58, this conference.

[9] J. Zhang, A. Alexander, and E. Simakov, "Fabrication of semiconductor photocathodes at ACERT", presented at the IPAC'24, Nashville, TN, USA, May 2024, paper WEPC54, this conference.

[10] A. Alexander, T. P. Grumstrup, H. Xu, and E. Simakov, "Design and construction of the photocathode vacuum suitcase for CARIE test facility", presented at the IPAC'24, Nashville, TN, USA, May 2024, paper MOPR83, this conference.